J Mol Model (2017) 23: 139
DOI 10.1007/s00894-017-3277-0

ORIGINAL PAPER

Reaction mechanisms of DNT with hydroxyl radicals for advanced oxidation processes—a DFT study

Yang Zhou[1,2] · **Zhilin Yang**[1] · **Hong Yang**[1,3] · **Chaoyang Zhang**[1] · **Xiaoqiang Liu**[2]

Received: 13 November 2016 / Accepted: 6 February 2017 / Published online: 29 March 2017

Abstract In advanced oxidation processes (AOPs), the detailed degradation mechanisms of a typical explosive of 2,4-dinitrotoluene (DNT) can be investigated by the density function theory (DFT) method at the SMD/M062X/6-311+G(d) level. Several possible degradation routes for DNT were explored in the current study. The results show that, for oxidation of the methyl group, the dominant degradation mechanism of DNT by hydroxyl radicals (•OH) is a series of sequential H-abstraction reactions, and the intermediates obtained are in good agreement with experimental findings. The highest activation energy barrier is less than 20 kcal mol^{-1}. Other routes are dominated by an addition-elimination mechanism, which is also found in 2,4,6-trinitrotoluene, although the experiment did not find the corresponding products. In addition, we also eliminate several impossible mechanisms, such as dehydration, HNO_3 elimination, the simultaneous addition of two •OH radials, and so on. The information gained about these degradation pathways is helpful in elucidating the detailed reaction mechanism between nitroaromatic explosives and hydroxyl radicals for AOPs.

Keywords 2,4-Dinitrotoluene · Degradation mechanism · DFT

✉ Yang Zhou
zhouy@caep.ac.cn

[1] Institute of Chemical Materials, Chinese Academy of Engineering and Physics, Mianyang 621900, China

[2] College of Chemistry and Environmental Engineering, Sichuan University of Science and Engineering, Zigong 643000, China

[3] School of Material Science and Engineering, Tsinghua University, Beijing 100084, China

Introduction

Environmental pollution by energetic compounds (explosives, propellants, and pyrotechnics) has become a global problem shared by many countries [1, 2]. Especially, pollution caused by TNT (2,4,6-trinitrotoluene) had been given more attention because of its high output and its identification in recent years as a class C carcinogen [3–10]. In comparison, less attention has been paid to DNT (2,4-dinitrotoluene). Comparing with TNT, DNT only needs to lose a nitro group to become the precursor of TNT synthesis, and DNT is also used as a plasticizing and gelatinizing agent or as a modifier for explosives and smokeless powders [11–13]. It is highly toxic to aquatic organisms, invertebrates, algae, and bacteria [14]. Therefore, the environmental impact of DNT is also a major public concern. For example, the US waste water treatment standard for DNT was determined as 0.32 mg/L for discharge to streams [15].

As a consequence, alternative methods for the removal of energetic compounds such as DNT have been considered, such as adsorption [16], alkaline hydrolysis [3, 4], biodegradation [17], and advanced oxidation processes (AOPs) [18–22]. Along with alkaline hydrolysis and biodegradation, AOPs have shown great promise as a method to remove DNT from various environments. For example, Bin et al. [18] checked the efficacy of five AOPs in degrading DNT and confirmed that ozonation and Fenton oxidation are the best choice. Celin et al. [19] testified to the efficiency of the photo-Fenton technique compared to photolysis and the photo-peroxide system for removing DNT in aqueous phase. Later, Chen et al. [20] also pointed out that the removal efficiency of Fenton oxidation is superior to that of the photo-peroxide method. Liou et al. [21] determined the sequence of oxidation efficiencies in Fenton system for several explosives including DNT. Phutane et al. [22] explored the removal of DNT from building-grade concrete. However, studies on the detailed

degradation mechanisms of DNT to date are still rare, except for the two possible pathways (denitration and oxidation) proposed by Chen et al. [20]. The oxidation mechanism is then further verified by detecting the intermediates [23, 24]. Clearly, a deficiency in knowledge of the detailed mechanisms will limit the development of new AOP technologies. Hence, the purpose of our study was to explore degradation mechanisms that include the structure of intermediates of DNT detected by experiments.

Considering the challenges of experiments involving seizing lively radicals and short-lived intermediates, quantum chemistry methods have become a good choice. Indeed, several works have used density function theory (DFT) to study the alkaline hydrolysis of energetic compounds [3, 4, 25, 26]. We also focused on the reaction mechanisms of TNT with •OH for AOPs by DFT [10]. However, relevant studies for DNT are rare. Here, we focus on the reaction mechanisms of DNT with •OH, because to study all reactions of AOPs by quantum chemistry methods simultaneously would be too complicated. Finally, we hope that our investigations will provide meaningful help for the understanding of the degradation process of DNT, and promote the development of AOP technologies for the removal of nitroaromatics.

Computational methods

All calculations were performed using the Gaussian 09 suite of programs [27]. The relevant stationary points in reaction pathways were fully optimized at the M062X/6-311+G* level [28, 29]. The solvent effect was described by the SMD solvent model [30]. Considering the actual environment, aqueous solution was chosen. We did not re-verify the reliability of the functional M062X and SMD model, since they had been used successfully to investigate the alkaline hydrolysis of several explosives including TNT, DNT, DNAN and RDX by Leszczynski's group [3, 4, 25]. All stationary points were further characterized by frequency analysis to be minima (all real frequencies) or transition states (TS; one and only one imaginary frequency). Additionally, zero-point vibrational energies, the corrections to enthalpy, entropy and Gibbs free-energy were also determined by calculation of the analytic harmonic vibrational frequencies at the same theory level as geometry optimization. The intrinsic reaction coordinates (IRC) [31] path was traced to check the energy profiles connecting each TS to the two associated minima of the proposed mechanism. The refined energies were corrected to enthalpies and free energies at 298.15 K and 1 atm, using the revised harmonic frequencies. Gibbs free energies of all considered species were calculated using standard expression: $\Delta G = \Delta H - T\Delta S$ at $T = 298.15$ K.

Results and discussion

AOPs are near-ambient-temperature water treatment processes that depend on the generation of radical species, mainly •OH radicals. Due to an unpaired electron in oxygen atom, •OH becomes a strong oxidizing agent (E^{o}=2.8 vs. ENH at pH 0) able to readily steal hydrogen atoms from other molecules to form water molecules, and contribute to unsaturated bonds [32]. The reactions of •OH radicals with organic compounds in aqueous solution are often complex chemical processes that proceed through a number of partially oxidized radical intermediates. However, the two initial reaction mechanisms, hydrogen (H) atom abstraction and addition to unsaturated bonds (double bond or aromatic ring), are still unequivocal [32]. Combined with the intermediates found by experiments [20, 22–24], we can roughly give the two reaction pathways of DNT (labelled as **0**) with •OH, as shown in Fig. 1. Then, we will gradually clarify how DNT is degraded by •OH radicals to 2,4-dinitrobenzaldehyde (**1**), 2,4-dinitrobenzoic acid (**2**), and mononitrotoluene (**4**), which are the products at the early stage of reactions.

Methyl group oxidation

For the initial steps of DNT reacting with •OH, a rough oxidation pathway for the methyl (CH_3) group, from DNT to 2,4- dinitrobenzoic acid via 2,4-dinitrobenzaldehyde (**0**→**1**→**2**), had been proposed by Chen et al. [20]. This route is very similar to that of TNT [10]. Similarly, it also lacks a number of crucial details on reaction mechanisms and intermediates, such as 2,4-dinitrobenzyl alcohol (named as **IN1**). In Fig. 2, we add the missing intermediates and TS information, referring to our knowledge of TNT [6, 7, 10]. In general, this pathway contains a series of H-abstraction and dehydration reactions, as shown in Fig. 2. Next, we gradually dissected this pathway by means of confirmation of the TSs and the data of reaction (ΔG_R) or activation (ΔG) Gibbs free energies.

In the first step, the •OH radical seizes an H atom from the CH_3 group of DNT, then generates a radical intermediate **R1** by **TS1**. Due to the asymmetry of **0** in Fig. 3, we checked the TSs, **TS1**, **TS1′** and **TS1″**, which correspond to three H atoms (labelled as **I**, **II**, **III**) of the CH_3 group, respectively. From Fig. 3, we can see that the lengths of the C–H breaking and H–O forming bonds are 1.20 and 1.34 Å at **TS1**, 1.21 and 1.33 Å at **TS1′**, and 1.22 and 1.31 Å at **TS1″**, respectively. This implies that the H-abstraction is an asynchronous atom-transfer reaction, and that the geometries of the TSs are closer to the reactants. From the activation energies ($\Delta G^{\ddagger}$ for solvent phase) in Fig. 3, we find that **TS1** has the lowest $\Delta G^{\ddagger}$ (9.1 kcal mol^{-1}), **TS1′** has a moderate $\Delta G^{\ddagger}$ (10.3 kcal mol^{-1}) and **TS1″** is the highest one (12.2 kcal mol^{-1}). This

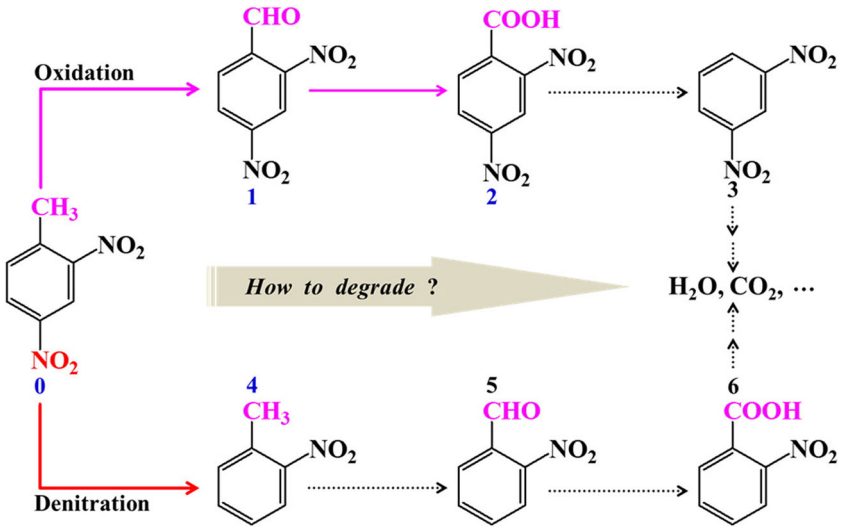

Fig. 1 Possible reaction pathway of mineralization of 2,4-dinitrotoluene (DNT) by Fenton oxidation

corresponds to the sequence of the distance between the O-atom of *ortho*-NO_2 group and the H-atom of •OH, which is 2.21 Å for **TS1**, 2.32 Å for **TS1′**, and 5.44 Å for **TS1″**, respectively. Therefore, we think that **TS1** and **TS1′** form weak hydrogen bonds that are conducive to H-abstraction reactions.

In Fig. 2, **R1** would further react with •OH without the barrier and form the 2,4-dinitrobenzyl alcohol (**IN1**), which has not been reported experimentally to date. However, the similar 2,4,6-trinitrobenzyl alcohol for AOPs of TNT had been detected by Ayoub et al. [7]. Next, **IN1** would pass through two routes to 2,4-dinitrobenzaldehyde (**1**). The first route is that •OH abstracts the H linked with C atom of CH_3OH group, then generates the radical **R2** through **TS2. R2** subsequently combines with •OH and forms the compound **IN2**. The second one is that •OH attacks the H at the O (not C) atom of CH_3OH group and forms the compound **IN2′**. Like **IN1**, both **IN2** and **IN2′** have also not been reported experimentally. From **IN2** (or **IN2′**) to **1** (found by experiment [20, 24]), the transformation is a dehydration reaction process through **TS3** (or **TS3′**). The last step from **1** to **R3** through **TS4** is also an H-abstraction reaction, and results in the generation of another detected intermediate **2** by the addition of another •OH. The TS geometries of the above reactions are given in Fig. 4.

TS2, **TS2′** and **TS4** are the TSs of H-abstraction reactions, and **TS3** and **TS3′** are the TSs of the dehydration reaction. Figure 4 shows that **TS3** differs slightly from the others. The H···•OH distance (1.15 Å) is less than that of H···O•CHR (1.38 Å), indicating that the **TS3** is closer to the product. However, other TSs, such as **TS2**, **TS2′**, **TS3′**, and **TS4**, are closer to the reactant. Calculated reaction (ΔG_R) and activation (ΔG) Gibbs free energies for all routes in Fig. 2 are listed in Table 1. The first H-abstraction (**0**+•OH→**TS1**→**R1**+H_2O) reaction has a lower energy barrier of 9.1 kcal mol^{-1} in water. Similarly, the last H-abstraction (**1**+•OH→**TS4**→**R3**+H_2O) has an almost identical $\Delta G^{\ddagger}$ of 9.2 kcal mol^{-1}. As for the second H-abstraction, **IN1**+•OH→**TS2′**→**IN2′**+H_2O has a higher $\Delta G^{\ddagger}$ of 13.8 kcal mol^{-1}, which is approximately twice as much as that of **IN1**+•OH→**TS2**→**IN2**+H_2O (7.0 kcal mol^{-1}), hinting that the latter is preferred. Interestingly, the two dehydration reactions of **IN2**→**TS3**→**1**+H_2O and **IN2′**→**TS3′**→**1**+H_2O have rather high activation

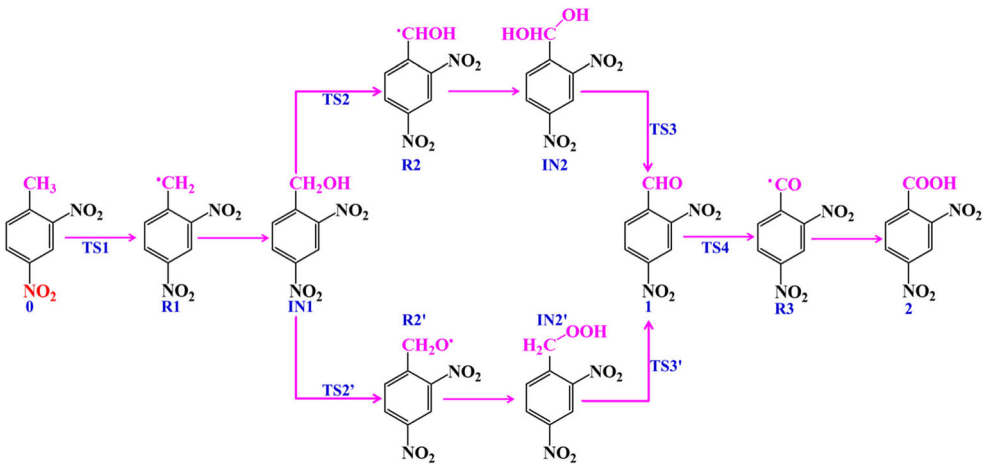

Fig. 2 Oxidation mechanisms of the methyl group for the degradation reaction of DNT only by •OH radicals

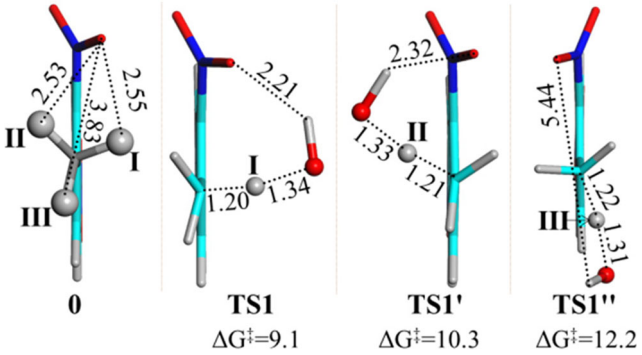

Fig. 3 Optimized geometries of **TS1**, **TS1′** and **TS1″** for the first H-abstraction reaction of DNT, with the selected distance given in Å. The activation energy is given in kcal mol^{-1}

barriers of about 40.0 kcal mol^{-1} and 57.4 kcal mol^{-1}, respectively. Table 1 also shows that all reactions involved in oxidations of CH_3 for DNT are exothermic, except for **IN2**→**TS3**→**1**+H_2O in gas phase (ΔG_R=1.5 kcal mol^{-1}). The Hammond-Leffler postulate predicts that TSs should resemble the reactant in exothermic reactions, and the product in endothermic reactions. Hence, we can infer that **TS3** should closely resemble the product, and other TSs (**TS1**, **TS2**, **TS2′**, **TS3′**, and **TS4**) should resemble the reactants. Indeed, this is in agreement with the above analysis for TS geometries. On the whole, the four H-abstraction reactions have lower activation barriers, <20 kcal mol^{-1}, which can occur easily at room temperature. However, the two dehydration reactions have the high activation barriers, and the influence of solvation on activation barriers is not noticeable. If this pathway is true, the compound **IN2** or **IN2′** should be detected by experiment; nevertheless, there are no corresponding reports. Evidently, other possible pathways are still hidden.

Next, we designed another two routes of **R2**+•OH→**TS5**→**1**+H_2O and **R2′**+•OH→**TS5′**→**1**+H_2O, i.e., the radical intermediates **R2** or **R2′** further abstract an H-atom by •OH but not coupled with •OH. The relative free energetic surface and key geometric parameters are displayed in Fig. 5. It is clear that the two new H-abstraction reactions are highly exothermic, $\Delta G_R^{\ddagger}$ = −71.3 kcal mol^{-1} and −94.9 kcal mol^{-1}, respectively. For **R2**, •OH can abstract the H-atom at the oxygen atom, finally forming **TS5**. This reaction has an activation barrier of 16.6 kcal mol^{-1}, which is higher than the earlier H-abstraction reactions (**IN1**→**TS2**→**R2** with 7.0 kcal mol^{-1} and **0**→**TS1**→**R1** with 9.1 kcal mol^{-1}). For **R2′**, the H-abstraction reaction has a barrier of 11.3 kcal mol^{-1}, slightly higher than the first one (**0**→**TS1**→**R1**, 9.1 kcal mol^{-1}) and lower than the second one (**IN1**→**TS2′**→**R2′**, 13.8 kcal mol^{-1}). Obviously, the activation energy barrier of new two routes shown in Fig. 5 is far less than those of two dehydration reactions (40 kcal mol^{-1} and 57.4 kcal mol^{-1}). Therefore, from the point of view of thermodynamics, they should be the main channel that results in the formation of 2,4-dinitrobenzaldehyde (**1**) directly from **IN1** (considering that the radical **R2** or **R2′** has an extremely short life time). In this way, we can explain why experiments [20, 24] often detected the intermediate 2,4-dinitrobenzaldehyde (**1**), rather than the intermediates **IN2** and **IN2′**.

Addition-elimination reaction

For aromatic compounds, •OH addition to an aromatic ring usually prevails over H abstraction when competition is possible, since the former is a negative energetic barrier process [32]. Therefore, we also proposed the reactions of •OH addition to different C-atoms of the DNT ring (labelled **I**–**VI**). The

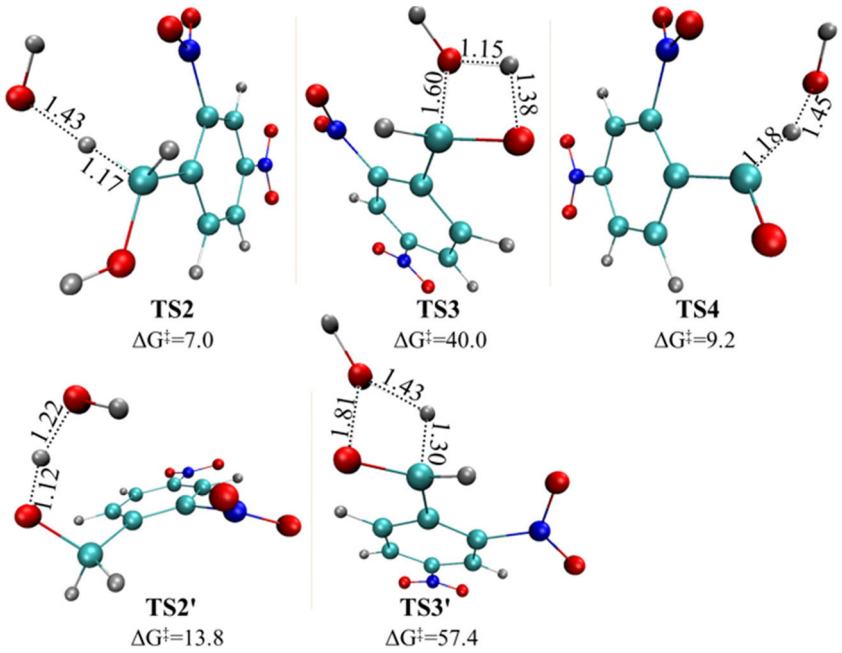

Fig. 4 Optimized geometries of **TS2**, **TS2′**, **TS3**, **TS3′**, and **TS4**, with the selected distance given in Å. The activation energy is given in kcal mol^{-1}

Table 1 Reaction (ΔG_R and $\Delta G_R^{\ddagger}$ for gas and solvent phase, respectively) and activation (ΔG and $\Delta G^{\ddagger}$ for gas and solvent phase, respectively) Gibbs free energies at 298.15 K for all reactions in Fig. 2 (kcal mol^{-1})

Reaction step[a]	ΔG_R	$\Delta G_R^{\ddagger}$	ΔG	$\Delta G^{\ddagger}$
0+•OH→**TS1**→**R1**+H_2O	−22.0	−25.6	9.2	9.1
IN1+•OH→**TS2**→**R2**+H_2O	−33.9	−38.4	5.9	7.0
IN1+•OH→**TS2′**→**R2′**+H_2O	−12.8	−14.8	11.7	13.8
IN2→**TS3**→**1**+H_2O	1.5	−5.2	43.3	40.0
IN2′→**TS3′**→**1**+H_2O	−58.9	−66.5	56.1	57.4
1+•OH→**TS4**→**R3**+H_2O	−58.4	−61.8	6.6	9.2

[a] The compounds represented by the notations are the same as those in Figs. 1 and 2

corresponding results are plotted in Fig. 6. As shown in Fig. 6, we gave the entire possible pathways, mainly considering the detected products of 1,3-dinitrobenzene (**3**) and mononitrotoluene with two isomers (**4** or **4′**). For example, **R4** from •OH addition to the **I** position of the ring is followed by the elimination of CH_3OH, and generates a radical **R5**. If **R5** continues to react with •H, the detected product **3** would be obtained. If **R4** eliminates a HNO_3, another detected product **4** would be produced by the further neutralization of •H. To check the probability of these reactions in Fig. 6, their reaction Gibbs free energies in gas and aqueous phase are summarized in Table 2. The data listed in Table 2 shows that all the reactions are endergonic. In detail, the reactions, including the elimination of CH_3OH, have the relatively lower $\Delta G_R^{\ddagger}$ of 22.9 and 17.7 kcal mol^{-1} for **R4**→**R5** and **R12**→**R5** in aqueous, respectively. Based on TS theory, we know that the activation energy barriers ($\Delta G^{\ddagger}$) should be higher than these values. From Fig. 6, we can also see that these two reactions

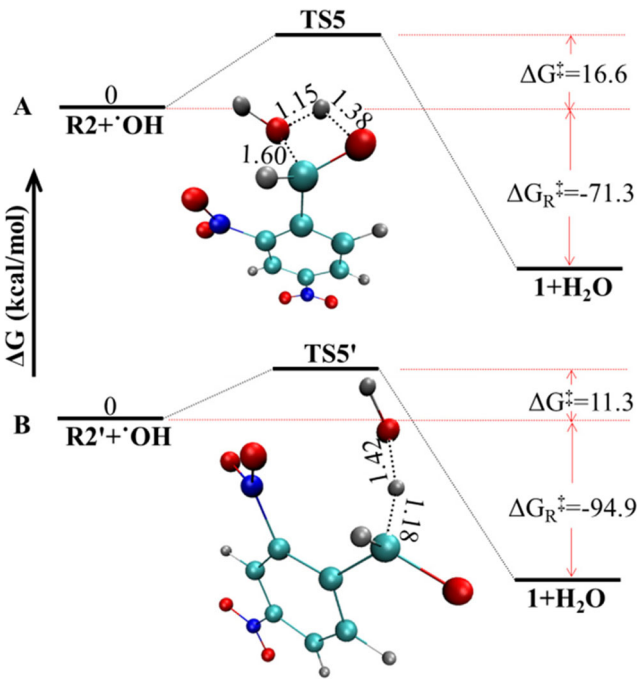

Fig. 5 Free energy profile and geometries of TSs for other H-abstraction reactions including two radicals. The selected distances in **TS5** and **TS5′** are given in Å

are related to the product **3** detected by experiments [20, 23]. However, in experiments, the proposed pathway for **3** was generally oxidation of the methyl group. In the above analysis, our proposed sequential H-abstraction reactions with the lower barrier, not the addition-elimination mechanism, should be responsible for the production of **3**. In addition, those processes involving the elimination of HNO_3 have the higher $\Delta G_R^{\ddagger}$ of 39.3 kcal mol^{-1}, 43.8 kcal mol^{-1}, 41.5 kcal mol^{-1}, 44.7 kcal mol^{-1}, 44.2 kcal mol^{-1}, and 43.6 kcal mol^{-1} (see Table 2), respectively, which are approximately twice as high as the $\Delta G_R^{\ddagger}$ of reactions with the elimination of CH_3OH. For these endoergic reactions with the elimination of HNO_3, $\Delta G^{\ddagger}$ would be greater than $\Delta G_R^{\ddagger}$. Hence, the $\Delta G^{\ddagger}$ of these six reactions should be far more than 20 kcal mol^{-1}, which indicates that these reactions are not feasible at room temperature.

It is worth noting that there are two unusual routes, involving the elimination of •NO_2 after •OH addition (**R7**-•NO_2→**IN4** and **R8**-•NO_2→**IN5**). Taking the reaction of **R7**-•NO_2→**IN4** as an example, the further result gives an activation barrier of 0.7 kcal mol^{-1}. This is close to zero and far less than that of CH_3OH and HNO_3 elimination. Clearly, the addition-elimination with •NO_2 should be the easiest reaction channel. This addition-elimination mechanism is also found for TNT [10], and the substituent pathway (i.e., addition-elimination) is very common in the case of aromatic rings [32]. However, the corresponding products **IN4** and **IN5** have not been reported by any experiments. Maybe, the subsequent degradation of **IN4** and **IN5** is also a very fast reaction process. Of course, this requires further theoretical or experimental investigation. On the other hand, from the above analysis we know that our proposed addition-elimination mechanisms cannot generate the product of mononitrotoluene (**4**) detected by Chen et al. [20]. We also checked the addition reaction of two •OH radicals, which also involve the elimination of CH_3OH and HNO_3 with higher barriers (about 80.2 kcal mol^{-1} and 72.4 kcal mol^{-1}, respectively). Therefore, these results are not given here. Because the nitro group is subject to isomerization reactions that, instead of –NO_2 by –ONO or –OON, we think that elimination of NO_2 should start from isomerization. Therefore, in the following works, we will investigate the relationship

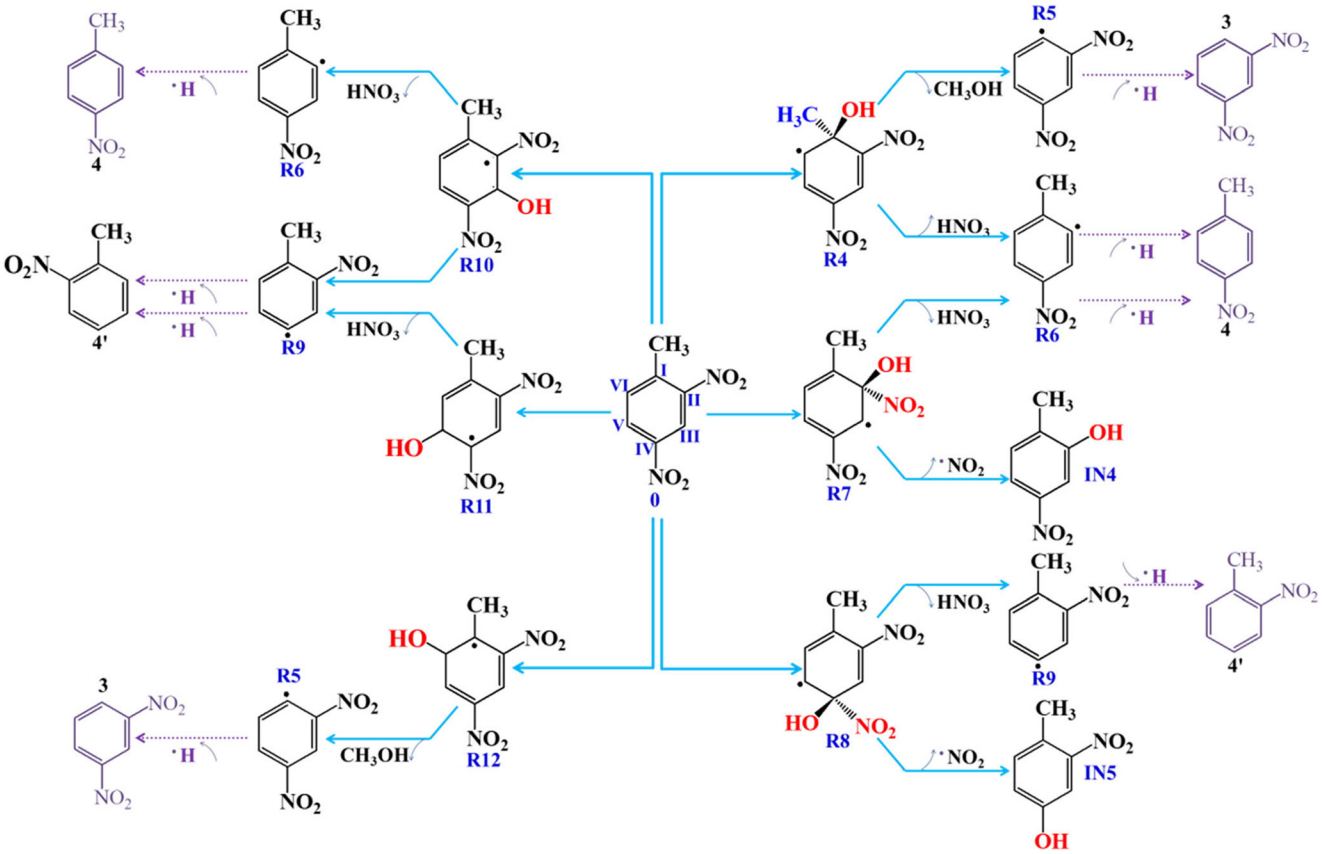

Fig. 6 Addition-elimination mechanisms for the degradation reaction of DNT only by •OH radicals

between the denitration and isomerization of NO_2 for more nitroaromatic explosives.

Comparison

We have shown the possible pathways of DNT degradation by comparing experimental results [20, 23, 24] and our simulations for TNT [10], which includes oxidation of the methyl group and addition-elimination reactions. The corresponding potential energy surfaces (PESs) for these two pathways are summarized in Figs. 7 and 8, respectively. In summary, oxidation of the methyl group mainly includes the mechanism of H-abstraction and contains two routes: the first is one H-abstraction followed by one dehydration reaction, and the highest activation barriers are of 40.0 kcal mol^{-1} and 57.6 kcal mol^{-1}, as shown in Fig. 7 (gray). The second is three continuous steps of H-abstraction reaction (see Fig. 7, red and blue), with activation barriers of 16.6 kcal mol^{-1} (highest) and 7.0 kcal mol^{-1} (lowest) (also see Fig. 5), respectively. Comparing the results of the two routes clearly shows that the detected products of 2,4-dinitrobenzaldehyde (**1**), 2,4-dinitrobenzoic acid (**2**), and 1,3-dinitrobenzene (**3**) [20, 23, 24] should be involved in the second route, i.e., three sequential steps of H-abstraction reaction. Therefore, we not only verified the pathway proposed by Chen et al. [20], but also detailed this pathway, providing radical intermediates and TSs.

The addition-elimination mechanism of •OH adding to aromatic ring also contains three routes: the first is the elimination of CH_3OH and HNO_3 after one •OH addition to the benzene ring. These reactions are endothermic and

Table 2 Reaction (ΔG_R and $\Delta G_R^{\ddagger}$ for gas and solvent phase, respectively) Gibbs free energies at 298 K for all reaction processes in Fig. 6 (kcal mol^{-1})

Reactions[a]	ΔG_R	$\Delta G_R^{\ddagger}$	Reactions	ΔG_R	$\Delta G_R^{\ddagger}$
R4-CH_3OH→**R5**	24.4	22.9	**R4**-HNO_3→**R6**	38.8	39.3
R7-HNO_3→**R6**	42.8	43.8	**R8**-HNO_3→**R9**	42.0	44.2
R10-HNO_3→**R6**	36.9	41.5	**R10**-HNO_3→**R9**	40.4	44.7
R11-HNO_3→**R9**	40.2	43.6	**R12**-CH_3OH→**R5**	18.3	17.7

[a] The compounds represented by the notations can be seen in Fig. 6

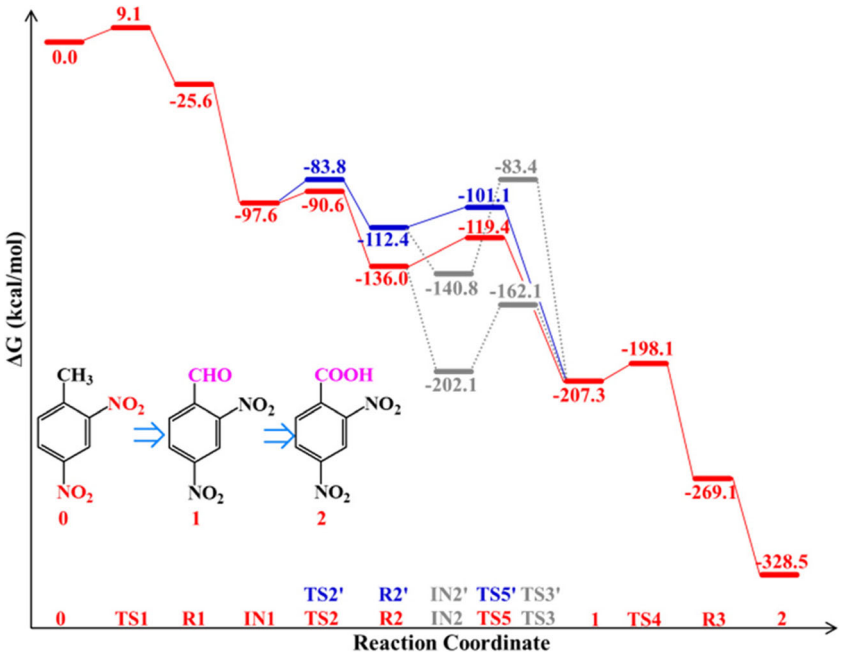

Fig. 7 Relative ΔG potential energy surfaces (PES) for the oxidation of methyl group (kcal mol^{-1}). The compounds represented by the notations can be seen in Figs. 1–5

the estimated activation barriers are far more than 20 kcal mol^{-1} based on the ΔG_R data in Table 2, as shown in Fig. 8. The second is the elimination of CH_3OH and HNO_3 after two •OH radicals addition to different positions of the ring. These routes have the highest activation barriers of 80.2 kcal mol^{-1} and 72.4 kcal mol^{-1} in all proposed pathways of DNT degradation in this work. The third route is the addition-elimination mechanism, that is, •OH addition to the ring followed by the elimination of •NO_2; this has a barrier of 0.7 kcal mol^{-1} (Fig. 8, red), which is the lowest in all the proposed pathways of DNT degradation. Evidently, the last route (addition-elimination) should also be a main reaction channel. However, the products of 2-hydroxyl-4-nitrotoluene and 4-hydroxyl-2-nitrotoluene (see Fig. 8) have still not been detected by experiment. In addition, the mechanism of NO_2 isomerization will be addressed in our next investigations.

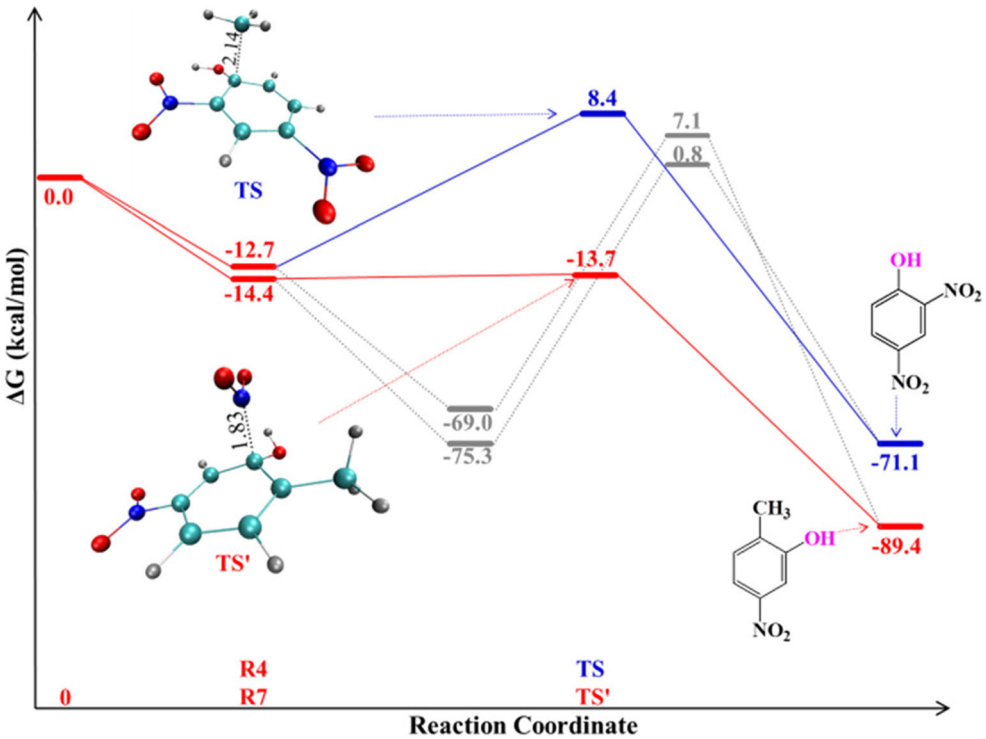

Fig. 8 Relative ΔG PES for addition-elimination reactions (kcal mol^{-1}). The compounds represented by the notations can be seen in Fig. 6

Conclusions

In this work, we investigated the degradation reactions with hydroxyl radicals in AOPs for the important nitroaromatic explosive 2,4-dinitrotoluene (DNT) by means of DFT methods at the M06-2X/6-311+G(d) level. The results show that the dominant pathway of DNT degradation is sequential H-abstraction and addition-elimination reactions. Sequential H-abstraction reactions can well explain the intermediates detected by several experiments [20, 23, 24]. Addition-elimination reactions should be also regarded as the main channel of DNT degradation based on the lowest activation barriers (0.7 kcal mol^{-1}), which is similar to TNT [10], and very common in the other case of aromatic ring [32], although the intermediates produced were not reported. Details of TSs, intermediate radicals and free energy surfaces for all proposed reactions are also given to make up for the lack of experimental knowledge. In addition, the influence of solvation on the degradation reactions is also provided. Given the lack of experimental data, we provided information of degradation pathways that are crucial if we are to understand the detailed reaction mechanism between nitroaromatic explosives and hydroxyl radicals for AOPs.

Acknowledgments All the authors appreciate very much the financial support from National Nature Sciences Foundation of China (No.11402241) and Foundation of Council for the Accreditation of Educator Preparation (CAEP) (No. 2014-1-075).

References

1. Pichtel J (2012) Distribution and fate of military explosives and propellants in soil: a review. Appl Environ Soil Sci 2012:617236
2. Sunahara GI, Lotufo GR, Kuperman RG, Hawari J (2009) Ecotoxicology of explosives. Taylor & Francis Group, CRC, Boca Raton
3. Hill FC, Sviatenko LK, Gorb L, Okovytyy SI, Blaustein GS, Leszczynski J (2012) DFT M06-2X investigation of alkaline hydrolysis of nitroaromatic compounds. Chemosphere 88:635–643
4. Sviatenko LK, Kinney C, Gorb L, Hill FC, Bednar AJ, Okovytyy SI, Leszczynski J (2014) Comprehensive investigations of kinetics of alkaline hydrolysis of TNT (2,4,6-trinitrotoluene), DNT (2,4-dinitrotoluene), and DNAN (2,4-dinitroanisole). Environ Sci Technol 48:10465–10474
5. Ayoub K, van Hullebusch ED, Cassir M, Bermond B (2010) Application of advanced oxidation processes for TNT removal: a review. J Hazard Mater 178:10–28
6. Ayoub K, Nelieu S, van Hullebusch ED, Grondard AM, Cassir M, Bermond A (2011) TNT oxidation by Fenton reaction: reagent ratio effect on kinetics and early stage degradation pathways. Chem Eng J 173:309–317
7. Ayoub K, Nelieu S, van Hullebusch ED, Labanowski J, Afonso IS, Bermond A, Cassir M (2011) Electro-Fenton removal of TNT: evidences of the electro-chemical reduction contribution. Appl Catal B Environ 104:169–176
8. Yardin G, Chiron S (2006) Photo-Fenton treatment of TNT contaminated soil extract solutions obtained by soil flushing with cyclodextrin. Chemosphere 62:1395–1402
9. Chen WS, Liang JS (2009) Electrochemical destruction of dinitrotoluene isomers and 2, 4, 6-trinitrotoluene in spent acid from toluene nitration process. J Hazard Mater 161:1017–1023
10. He X, Zeng Q, Zhou Y, Zeng QX, Wei XF, Zhang CY (2016) A DFT study toward the reaction mechanisms of TNT with hydroxyl radicals for advanced oxidation processes. J Phys Chem A 120: 3747–3753
11. Tchounwou PB, Newsome C, Glass K, Centeno JA, Leszczynski J, Bryant J, Okoh J, Ishaque A, Brower M (2003) Environmental toxicology and health effects associated with dinitrotoluene exposure. Rev Environ Health 18:203–229
12. Shin KH, Lim Y, Ahn JH, Khil J, Cha CJ, Hur HG (2005) Anaerobic biotransformation of dinitrotoluene isomers by Lactovovvus lactis subspecies lactis strain 27 isolated from earthworm intestine. Chemosphere 61:30–39
13. Patapas J, Al-Ansari MM, Taylor KE, Bewtra JK, Biswas N (2007) Removal of dinitrotoluenes from water via reduction with iron and peroxidase-catalyzed oxidative polymerization: a comparison between arthromyces ramosus peroxidase and soybean peroxidase. Chemosphere 67:1485–1491
14. Gong P, Kuperman RG, Sunahara GI (2003) Genotoxicity of 2,4- and 2,6-dinitrotoluene as measured by the tradescantia micronucleus (trad-MCN) bioassay. Mutat Res 38:13–18
15. Paca J, Halecky M, Barta J, Bajpai R (2009) Aerobic biodegradation of 2,4-DNT and 2,6-DNT: performance characteristics and biofilm composition changes in continuous packed-bed bioreactors. J Hazard Mater 163:848–854
16. Rajagopal C, Kapoor JC (2001) Development of adsorptive removal process for treatment of explosives contaminated wastewater using activated carbon. J Hazard Mater 87:73–98
17. Kuscu D, Sponza T (2011) Application of Box-Wilson experimental design method for 2, 4-dinitrotoluene treatment in a sequential anaerobic migrating blanket reactor (AMBR)/aerobic completely stirred tank reactor (CSTR) system. J Hazard Mater 187:222–234
18. Bin AK, Machniewski P, Sakowicz R, Ostrowska J, Zielinski J (2001) Degradation of nitroaromatics (MNT, DNT and TNT) by AOPs. Ozone Sci Eng 23:343–349
19. Celin SM, Pandit M, Kapoor JC, Sharma RK (2003) Studies on photo-degradation of 2, 4-dinitrotoluene in aqueous phase. Chemosphere 53:63–69
20. Chen WS, Juan CN, Wei KM (2005) Mineralization of dinitrotoluenes and trinitrotoluene of spent acid in toluene nitration process by Fenton oxidation. Chemosphere 60:1072–1079
21. Liou MJ, Lu MC, Chen JN (2003) Oxidation of explosives by Fenton and photo-Fenton processes. Water Res 37:3172–3179
22. Phutane SR, Renner JN, Nelson SL, Seames WS, Paca J, Sundstrom TJ, Kozliak EI (2007) Removal of 2,4-dinitrotoluene from concrete using bioremediation, agar extraction, and photocatalysis. Folia Microbiol 52:253–260
23. He Y, Zhao B, Hughes JB, Han SS (2008) Fenton oxidation of 2, 4- and 2, 6-dinitrotoluene and acetone inhibition. Front Environ Sci Eng China 2:326–332
24. Xiao H, Liu RP, Zhao X, Qu JH (2008) Enhanced degradation of 2, 4-dinitrotoluene by ozonation in the presence of manganese (II) and oxalic acid. J Mol Catal A Chem 286:149–155
25. Sviatenko LK, Gorb L, Hill FC, Leszczynska D, Okovytyy SI, Leszczynski J (2015) Alkaline hydrolysis of hexahydro-1,3,5-trinitro-1,3,5-triazine: M06-2X investigation. Chemosphere 134:31–38
26. Salter-Blanc AJ, Bylaska EJ, Ritchie JJ, Tratnyek PG (2013) Mechanisms and kinetics of alkaline hydrolysis of the energetic nitroaromatic compounds 2, 4, 6-trinitrotoluene (TNT) and 2, 4-dinitroanisole (DNAN). Environ Sci Technol 47:6790–6798
27. Frisch MJ, Trucks GW, Schlegel HB, Scuseria GE, Robb MA, Cheeseman JR, Scalmani G, Barone V, Mennucci B, Petersson GA, Nakatsuji H, Caricato M, Li X, Hratchian HP, Izmaylov AF, Bloino J, Zheng G, Sonnenberg JL, Hada M, Ehara M, Toyota K,

Fukuda R, Hasegawa J, Ishida M, Nakajima T, Honda Y, Kitao O, Nakai H, Vreven T, Montgomery JA, Peralta JE, Ogliaro F, Bearpark M, Heyd JJ, Brothers E, Kudin KN, Staroverov VN, Kobayashi R, Normand J, Raghavachari K, Rendell A, Burant JC, Iyengar SS, Tomasi J, Cossi M, Rega N, Millam JM, Klene M, Knox JE, Cross JB, Bakken V, Adamo C, Jaramillo J, Gomperts R, Stratmann RE, Yazyev O, Austin AJ, Cammi R, Pomelli C, Ochterski JW, Martin RL, Morokuma K, Zakrzewski VG, Voth GA, Salvador P, Dannenberg JJ, Dapprich S, Daniels AD, Farkas O, Foresman JB, Ortiz JV, Cioslowski J, Fox DJ (2009) Gaussian 09, Revision A.01. Gaussian, Wallingford

28. Zhao Y, Truhlar DG (2008) The M06 suite of density functionals for main group thermochemistry, thermochemical kinetics, noncovalent interactions, excited states, and transition elements: two new functionals and systematic testing of four M06-class functionals and 12 other functionals. Theor Chem Accounts 120:215–241
29. McLean AD, Chandler GS (1980) Contracted Gaussian basis sets for molecular calculations. I. Second row atoms, Z=11-18. J Chem Phys 72:5639–5648
30. Marenich AV, Cramer CJ, Truhlar DG (2009) Universal solvation model based on solute electron density and on a continuum model of the solvent defined by the bulk dielectric constant and atomic surface tensions. J Phys Chem B 113:6378–6396
31. Hratchian HP, Schlegel HP (2004) Accurate reaction paths using a hessian based predictor-corrector integrator. J Chem Phys 120: 9918–9924
32. Gligorovski S, Strekowski R, Barbati S, Vione D (2015) Environmental implications of hydroxyl radicals (OH). Chem Rev 115:13051–13092